ADVANCED FUNCTIONAL MATERIALS
www.afm-journal.de

Synthesis and Structure–Property Correlations of Dicyanovinyl-Substituted Oligoselenophenes and their Application in Organic Solar Cells

Stefan Haid, Amaresh Mishra, Matthias Weil, Christian Uhrich, Martin Pfeiffer, and Peter Bäuerle**

The convergent synthesis of a series of acceptor–donor–acceptor (A-D-A) type dicaynovinyl (DCV)-substituted oligoselenophenes DCV*n*S (*n* = 3–5) is presented. Trends in thermal and optoelectronic properties are studied, in dependence on the length of the conjugated backbone. Optical measurements reveal red-shifted absorption spectra and electrochemical investigations show lowering of the lowest unoccupied molecular orbital (LUMO) energy levels for DCV*n*S compared to the corresponding thiophene analogs DCV*n*T. As a consequence, a lowering of the bandgap is observed. Single crystal X-ray structure analysis of tetramer DCV4S provides important insight into the packing features and intermolecular interactions of the molecules, further corroborating the importance of the DCV acceptor groups for the molecular ordering. DCV4S and DCV5S are used as donor materials in planar heterojunction (PHJ) and bulk-heterojunction (BHJ) organic solar cells. The devices show very high fill factors (FF), a high open circuit voltage, and power conversion efficiencies (PCE) of up to 3.4% in PHJ solar cells and slightly reduced PCEs of up to 2.6% in BHJ solar cells. In PHJ devices, the PCE for DCV4S almost doubles compared to the PCE reported for the oligothiophene analog DCV4T, while DCV5S shows an about 30% higher PCE than DCV5T.

1. Introduction

In contrast to oligothiophenes, oligoselenophenes are still a rather unexplored class of organic π-conjugated materials. This is mainly due to the less developed chemistry and higher price of selenophene. Therefore, some studies focused only on the theoretical investigation of oligoselenophenes.[1–4] The synthesis of a series of oligoselenophenes up to a hexamer was first published by Nakanishi et al. in 1997.[5,6] The authors showed that oligoselenophenes could be synthesized by the same C–C cross coupling reactions as oligothiophenes. Furthermore, the systematic changes of the optoelectronic properties in a series of oligoselenophenes were similar to those for oligothiophenes. The investigated oligoselenophenes exhibited red-shifted absorption spectra and lower bandgaps compared to their oligothiophene analogs. To date, this series remained the only systematically investigated series of oligoselenophenes.

Polyselenophenes, on the other hand, have been investigated more widely in recent years, both theoretically and experimentally. Some promising properties, especially for application in organic solar cells (OSC), were predicted and confirmed by experiments, i.e., lower bandgaps, red-shifted absorption and better polarizability compared to polythiophenes.[1,2,7–11] Due to the predicted favorable properties, several polyselenophenes and selenophene containing co-polymers have been applied in OSCs in the last few years and power conversion efficiencies of up to 6.87% were achieved.[12–20] Selenophene-based oligomers, on the other hand, have only scarcely been used in solar cells. Some selenophene-containing sensitizers for dye-sensitized solar cells were investigated.[21,22] A series of selenophene- and biselenophene-substituted diketopyrrolopyrroles was used in solution-processed bulk-heterojunction (BHJ) solar cells, whereby PCEs of 1.5% were achieved.[23] To the best of our knowledge, oligoselenophenes longer than a trimer have not been implemented in organic solar cells so far.

During the past years, the emergence of novel strategies in the design of conjugated small molecules and oligomers as well as the development of new device architectures has led to remarkable improvements in the performance of OSCs.[24] In our group, a number of acceptor-donor-acceptor (A-D-A) oligothiophenes have been synthesized and studied in vacuum-processed solar cells.[25–35] In particular, dicyanovinyl (DCV)-substituted oligothiophenes showed very good efficiencies,

S. Haid, Dr. A. Mishra, Prof. P. Bäuerle
Institute of Organic Chemistry II and Advanced Materials
University of Ulm
Albert-Einstein-Allee 11, D-89081 Ulm, Germany
E-mail: amaresh.mishra@uni-ulm.de;
peter.baeuerle@uni-ulm.de
Dr. M. Weil
Institut für Chemische Technologien und Analytik
Abteilung Strukturchemie, Technische Universität Wien
Getreidemarkt 9/164-SC, 1060 Vienna, Austria
Dr. C. Uhrich, Dr. M. Pfeiffer
Heliatek GmbH, Treidlerstr. 3, 01139 Dresden, Germany

DOI: 10.1002/adfm.201201018

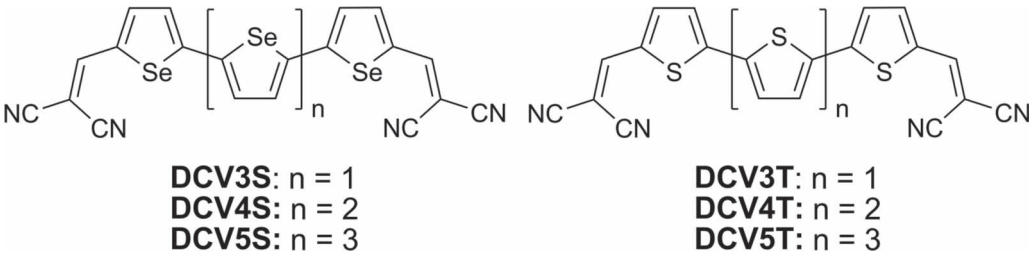

Scheme 1. Dicyanovinyl-substituted oligoselenophenes (left) and oligothiophenes (right).

and the best value of up to 5.2% was obtained with a DCV-substituted quinquethiophene (DCV5T) in BHJ solar cells.[27] In a very recent work, we investigated DCV-substituted selenophene-thiophene co-oligomers containing butyl side chains, which showed good PCEs of 2.5–3.0%.[28]

Encouraged by these results, we present now in this work the synthesis of a series of DCV-substituted oligoselenophenes **DCV*n*S**. Their thermal and optoelectronical properties and their application in OSCs will be discussed and compared to the previously reported oligothiophenes (**DCV*n*T**) (**Scheme 1**).[27] Furthermore, the single crystal structure analysis of the tetrameric **DCV4S** will be discussed and compared to its thiophene analog **DCV4T**.

2. Results and Discussion

2.1. Synthesis

The synthesis of **DCV3S** started with 2,2′:5′,2″-terselenophene **1**,[5] which was formylated in a Vilsmeier-Haack reaction with *N*,*N*-dimethylformamide (DMF)/phosphoryl chloride ($POCl_3$) to obtain dialdehyde **2** in 63% yield (**Scheme 2**). Dialdehyde **2** was reacted with malononitrile and β-alanine in a Knoevenagel condensation and after recrystallization from chlorobenzene **DCV3S** was obtained in 72% yield. Due to their expected low solubility, **DCV4S** and **DCV5S** were synthesized by a convergent approach developed recently in our laboratory.[27] Thus,

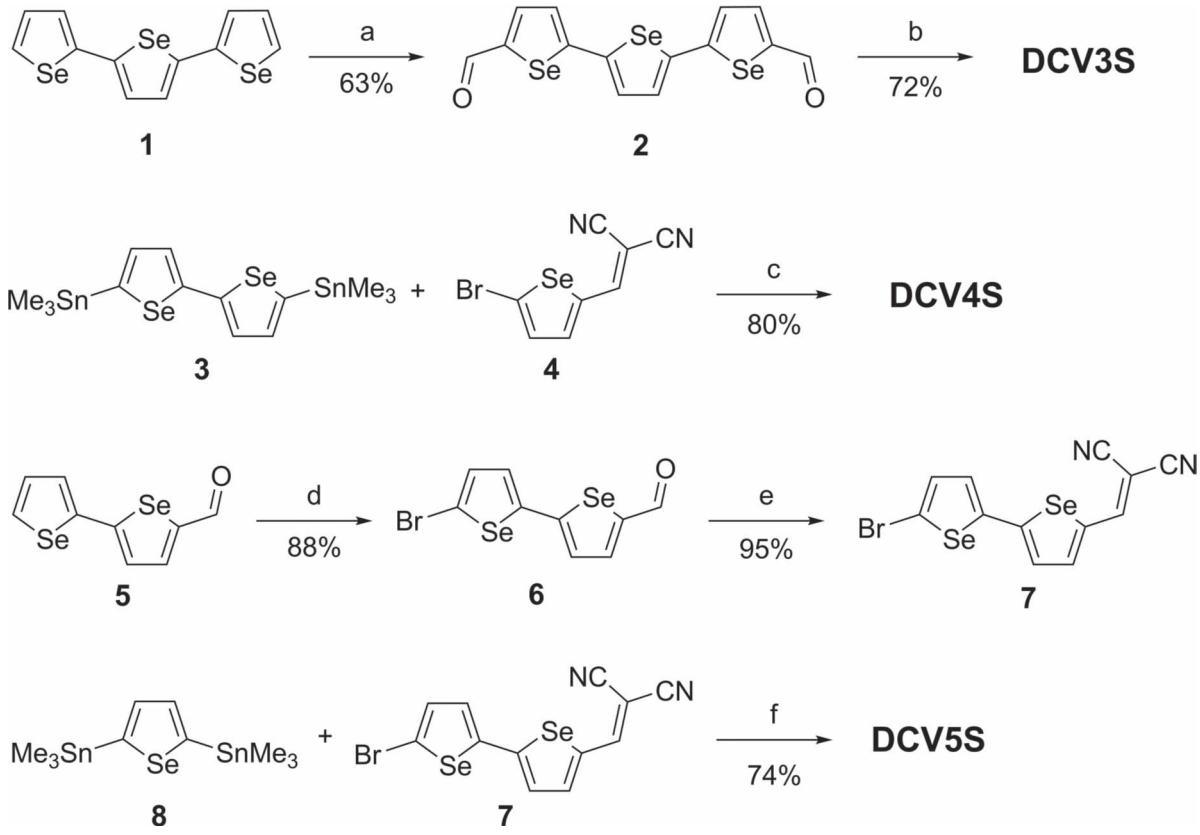

Scheme 2. a) $POCl_3$/DMF (20 equiv), dichloroethane, reflux, 5 d; b) malononitrile, β-alanine, dichloroethane/ethanol, reflux, 2 d; c) $Pd(PPh_3)_2Cl_2$, DMF, 80 °C, overnight; d) NBS (1 equiv), DMF, –25 °C, 3 d; e) malononitrile, β-alanine, dichloroethane/ethanol, reflux, 2 h; f) $Pd(PPh_3)_4$, DMF, 80 °C, overnight.

DCV4S was obtained by Stille cross-coupling of bisstannylated biselenophene **3**[36] and DCV-substituted bromoselenophene **4**[28] using $Pd(PPh_3)_2Cl_2$ as catalyst. After Soxhlet extraction with chlorobenzene, pure **DCV4S** was obtained in 80% yield. For the synthesis of **DCV5S**, DCV-substituted bromobiselenophene **7** was synthesized from 2,2′-biselenophene-5-carbaldehyde **5**[5] by monobromination with *N*-bromosuccinimide (NBS) in DMF at –25 °C, which afforded bromo derivative **6** in 88% yield. Subsequent Knoevenagel condensation with malononitrile gave diselenophene **7** in 95% yield. Stille cross-coupling of **7** with 2,5-bis(trimethylstannyl)selenophene **8**, which had been synthesized from 2,5-dibromoselenophene[28] by lithiation with *n*-butyl lithium (*n*-BuLi) and subsequent quenching with trimethyltin chloride, afforded **DCV5S** in 74% yield after Soxhlet extraction with chlorobenzene.

2.2. Thermal Properties

Oligoselenophenes **DCV3S**-**DCV5S** were designed for application in vacuum-processed solar cells and therefore need to be stable at the higher temperatures used for thermal evaporation. This thermal stability was investigated by Differential Scanning Calorimetry (DSC) under an argon atmosphere (**Figure 1**). The DSC curve of each compound showed one endothermic peak indicating the melting point and one exothermic peak at higher temperatures, indicating beginning decomposition. The melting points for all three compounds (282–358 °C) are substantially higher than those of the corresponding oligothiophenes[27] (ΔT_m = 17–38 °C, see **Table 1**). The oligoselenophenes showed the same odd-even effect as the analogous oligothiophenes. As a consequence, we found a significantly higher melting point for even numbered **DCV4S** (358 °C) than for odd-numbered **DCV3S** (282 °C) and **DCV5S** (324 °C). The decomposition temperatures of all oligomers were above 370 °C, a temperature which typically is sufficient for vacuum sublimation.

2.3. Optical Spectroscopy

The optical properties of **DCV*n*S** were investigated by UV-vis absorption and emission spectroscopy in dichloromethane solution (**Figure 2**a). In Table 1, the data are summarized and

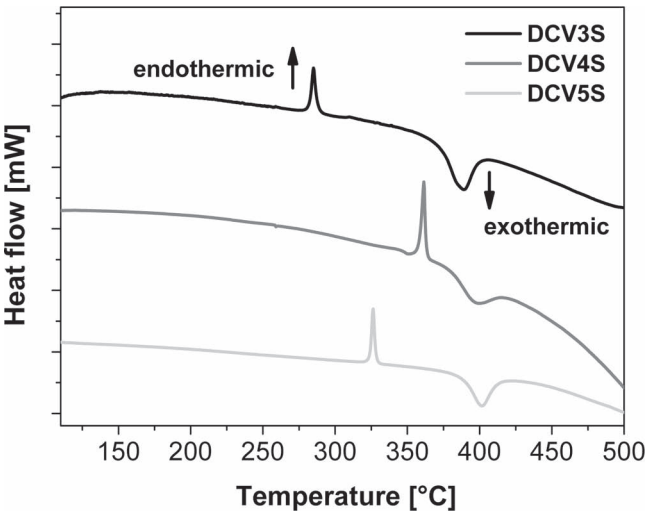

Figure 1. DSC curves for **DCV3S**-**DCV5S** measured under argon flow at a heating rate of 10 °C min^{-1}.

compared to the data for the corresponding oligothiophenes. The absorption spectrum of **DCV3S** showed a broad peak with a maximum at 521 nm. With increasing number of selenophene units, the absorption maximum is bathochromically shifted (**DCV4S**: $\lambda_{max,abs}$ = 547 nm; **DCV5S**: $\lambda_{max,abs}$ = 565 nm) due to extended π-conjugation. The emission spectrum of **DCV3S** clearly showed a structured band with a maximum at 599 nm and a vibronic shoulder at 638 nm. The spectra of **DCV4S** ($\lambda_{max,em}$ = 654 nm) and **DCV5S** ($\lambda_{max,em}$ = 695 nm) were red-shifted, but lost fine structure. Compared to the corresponding oligothiophenes (**DCV*n*T**), the absorption maxima are red-shifted by 25–35 nm. For the emission maxima, this trend is slightly more pronounced with shifts between 30 and 45 nm. In contrast to **DCV*n*T**, no clear trend for the molar extinction coefficients could be observed for **DCV*n*S**. The molar extinction coefficients of **DCV3S** (ε = 62 200 L mol^{-1} cm^{-1}) and **DCV5S** (ε = 63 500 L mol^{-1} cm^{-1}) are found to be in the same region. For **DCV4S**, however, no extinction coefficient could be determined because of its poor solubility.

Thin films were prepared for **DCV4S** and **DCV5S** by vacuum sublimation on glass substrates and their UV-vis absorption

Table 1. Optical data of **DCV*n*S** in comparison with their thiophene analogs **DCV*n*T**.

		solution			film		
Compound	T_m [a)] [°C]	λ_{abs} [nm]	λ_{em} [nm]	E_g^{opt} [b)] [eV]	λ_{abs} [nm]	λ_{em} [nm]	E_g^{opt} [c)] [eV]
DCV3S	282	521	599	2.08	–	–	–
DCV4S	358	547	654	1.95	581	797	1.68
DCV5S	324	565	695	1.89	596	822	1.60
DCV3T[d)]	265	495	564	2.20	528	695	1.85
DCV4T[d)]	320	518	612	2.09	560	670	1.78
DCV5T[d)]	287	530	663	2.02	570	767	1.69

[a)]Melting temperature determined from DSC; [b)]Estimated using the onset of the UV-vis spectra in DCM; [c)]Estimated using the onset of the thin film UV-vis spectra; [d)]Values taken from ref. [27].

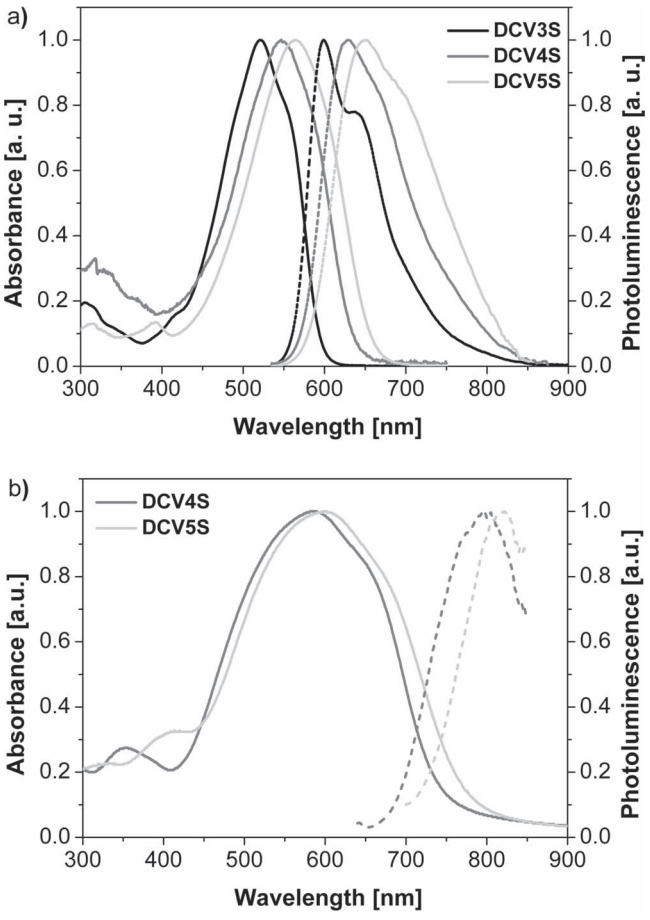

Figure 2. a) UV-vis absorption and emission spectra of **DCV3S**-**DCV5S** measured in dichloromethane. b) UV-vis absorption and emission spectra of **DCV4S** and **DCV5S** in thin films deposited by vacuum sublimation on glass substrates.

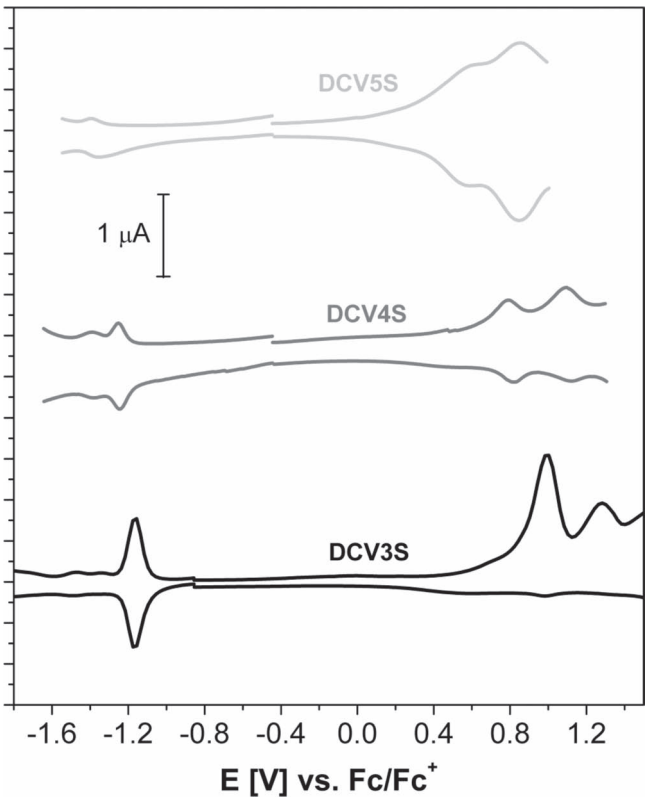

Figure 3. Differential pulse voltammograms of **DCV*n*S** measured in dichloromethane at 25 °C (**DCV3S**) or tetrachloroethane at 80 °C (**DCV4S**, **DCV5S**). Supporting electrolyte $TBAPF_6$ (0.1 M), scan rate 100 mV s^{-1}, potentials versus Fc/Fc^+.

and emission spectra were measured (Figure 2b). Compared to the solution spectra, the absorption spectra in thin films are significantly broadened and the maxima are bathochromically shifted by ≈30 nm due to planarization and ordering of the molecules in the solid state. The emission maxima are even further red-shifted by 130–140 nm. The broad and red-shifted absorptions result in reduced optical bandgaps for **DCV4S** and **DCV5S** compared to those in solution ($\Delta E_g^{opt} \approx 0.29$ eV). Both, in solution and in thin film, the bandgaps of the oligoselenophenes are by 0.1–0.15 eV lower than those of the corresponding oligothiophenes.

2.4. Electrochemical Characterization

The redox properties of **DCV3S** were measured by cyclic voltammetry (CV) and differential pulse voltammograms (DPV) at room temperature in dichloromethane solution with 0.1 M tetrabutylammonium hexafluorophosphate ($TBAPF_6$) as supporting electrolyte. Due to their poor solubility in dichloromethane, **DCV4S** and **DCV5S** were investigated in tetrachloroethane/$TBAPF_6$ solutions at 80 °C. All measurements were carried out with the ferrocene/ferrocenium couple as internal standard. DPVs of all three compounds are shown in **Figure 3**. The data are summarized and compared to the corresponding oligothiophenes in **Table 2**.

All three compounds showed one reduction and two oxidation processes. For **DCV4S**, a second reduction wave was visible. The oxidation potentials are shifted to more negative values with increasing chain length of the oligoselenophene. The first oxidation potential decreased from 0.99 V for **DCV3S** to 0.57 V for **DCV5S**, whereas the second one shifted from 1.28 V for **DCV3S** to 0.85 V for **DCV5S**. For the longer oligomers the redox waves are reversible, indicating the formation of stable radical cations and dications due to the extended conjugated system. Compared to the corresponding oligothiophenes, the oxidation potentials were lower by 0.1 V. The reduction potentials shifted as well to more negative values with increasing number of selenophenes (from –1.17 V for **DCV3S** to –1.38 V for **DCV5S**).

From the onset of the first oxidation and reduction potential, HOMO (highest occupied molecular orbital) and LUMO (lowest unoccupied molecular orbital) energy values were calculated for each compound by subtracting the respective value from the Fc/Fc^+ energy level (–5.1 eV vs. vacuum).[37] The difference of the thus determined HOMO and LUMO energies corresponds to the electrochemical bandgap (E_g^{CV}). The data are summarized in Table 2 and compared with the values for the oligothiophene analogs. The HOMO energy was raised with increasing number of selenophenes from –6.02 eV for **DCV3S** to –5.60 eV

Table 2. Electrochemical data for **DCV*n*S** compared to their thiophene analogs **DCV*n*T**.

compound	E^0_{ox1} [V]	E^0_{ox2} [V]	E^0_{red1} [V]	HOMO[a)] [eV]	LUMO[a)] [eV]	E_g^{CV} [eV]
DCV3S[b)]	0.99	1.28	–1.17	–6.02	–4.00	2.02
DCV4S[c)]	0.81	1.11	–1.25	–5.81	–3.96	1.85
DCV5S[c)]	0.57	0.85	–1.38	–5.60	–3.84	1.76
DCV3T[d)]	1.06	–	–1.25	–6.09	–3.90	2.19
DCV4T[d)]	0.84	1.20	–1.41	–5.85	–3.87	1.98
DCV5T[d)]	0.64	0.93	–1.37	–5.62	–3.73	1.89

[a)]Set Fc^+/Fc E_{HOMO} = –5.1 eV;[37] [b)]Measured in DCM/$TBAPF_6$ (0.1 M), 25 °C, V = 100 mV s^{-1}, vs. Fc^+/Fc; [c)]Measured in tetrachloroethane/$TBAPF_6$ (0.1 M), 80 °C, V = 100 mV s^{-1}, vs. Fc^+/Fc; [d)]Values according to ref. [27].

for **DCV5S**. For the LUMO energies we see the same trend, but somewhat smaller (–4.00 eV for **DCV3S** to –3.84 eV for **DCV5S**). Consequently, the electrochemical bandgap decreased from 2.02 eV for **DCV3S** to 1.76 eV for **DCV5S**. Compared to the oligothiophene analogs, the HOMO values of the oligoselenophenes are relatively similar while the LUMO values are lower by about 0.1 eV. Due to these lower LUMO energies, the electrochemical bandgap of the oligoselenophenes were 0.1–0.15 eV smaller compared to the oligothiophenes. The same trend was observed for the optical bandgaps (see above). The lower ionization potential[38] of selenium (9.75 eV) compared to sulfur (10.36 eV) could be the main reason for the lower LUMO energies of the investigated oligoselenophenes compared to their thiophene analogs. This is in accordance with theoretical studies, which have shown that upon replacement of sulfur by selenium the HOMO should remain relatively unaffected, whereas the LUMO should be stabilized by any heteroatom with a lower ionization potential.[39]

Due to the low HOMO energy of –6.02 eV, **DCV3S** rather shows an n-type semiconducting character and is not suitable as donor material in organic solar cells. On the other hand, **DCV4S** (E_{HOMO} = –5.81 eV) and **DCV5S** (E_{HOMO} = –5.60 eV) should be suitable p-type materials for OSCs with C_{60} as acceptor. The large difference between the HOMO of **DCV*n*S** and the LUMO of C_{60} (E_{LUMO} = –4.08 eV)[40] should provide reasonably high open circuit voltages (V_{OC}) as the V_{OC} depends mainly on the energy difference between the LUMO of the acceptor and HOMO of the donor materials.

2.5. Single Crystal Structure Analysis

Lath-like single crystals of **DCV4S** suitable for structural analysis were obtained after gradient sublimation at $1.75 \cdot 10^{-6}$ mbar and 325 °C. The crystals belong to the monoclinic space group $P2_1/n$ with 4 molecules in the unit cell. The unit cell parameters are: a = 3.92030(10), b = 27.6816(9), c = 22.7887(7) Å, β = 93.181(2)°. **Figure 4** shows the molecular structure of **DCV4S** in the crystal. The crystal structure is isostructural to that of the thiophene analog **DCV4T**.[27] The selenophene units show an all *trans* conformation while the DCV groups are in an all *cis* conformation relative to the selenium atoms of the adjacent selenophene ring. The configuration of the molecule is almost planar (rms deviation 0.116 Å) with dihedral angles between the selenophene units below 4.5°. The terminal DCV-groups are slightly twisted out of the molecular plane with nitrogen-plane distances of up to 0.33 Å.

The bond lengths of the oligoselenophene backbone are summarized in **Table 3** and the inter- and intramolecular non-bonding atom distances shorter than the sum of the corresponding van der Waals radii are collected in **Table 4**. The values for the selenophenic C=C double bonds (1.362–1.378 Å), C–C single bonds (1.402–1.409 Å) and the C–C interring bonds (1.438–1.446 Å) are comparable with those of the corresponding oligothiophene **DCV4T**. The C–Se bonds (1.872–1.892 Å), however, are substantially longer than the C–S bonds (1.730–1.745 Å) in **DCV4T** due to the larger selenium atom. These values are in good agreement with the values for the respective monomeric selenophene (1.855 Å) and thiophene (1.714 Å).[41,42]

The unit cell comprises four molecules divided into two centrosymmetric pairs of antiparallelly arranged molecules (**Figure 5**). In the crystal, molecules extend in layers parallel to the (9 3 21) plane with channels parallel to [100] that contain disordered molecules. It was not possible to resolve this disorder satisfactorily (for treatment of the disorder see details in the experimental section). Although the crystal structure looks very similar to that of **DCV4T**, some differences can be recognized by comparison of the intra- and intermolecular short contacts (Table 4 and Figure 4). Interestingly, no intramolecular short contacts between hydrogen and sulfur atoms are observed for **DCV4T**, while each selenium atom in **DCV4S** interacts with the hydrogen atoms of the adjacent selenophene ring(s). This is a consequence of the larger van der Waals radius of selenium (1.90 Å) compared to sulfur (1.80 Å).[43] In contrast to **DCV4T**, no intermolecular short distances between H2 and H11 are observed. However, there is an additional intermolecular interaction between Se3 and N2. For **DCV4T**, no intermolecular interactions between sulfur and nitrogen atoms were observed. The nitrogen atoms N2-N4 of **DCV4S** interact with hydrogens H7, H17 and H21 via weak non-classical C-H…N hydrogen bonds, but the bond lengths of the hydrogen bonds, especially the N2…H7 bond, are slightly larger compared to **DCV4T**, indicating slightly weaker hydrogen bonding.

DCV4S does not exhibit a herringbone structure in the crystal which was observed for the parent 2,2′:5′,2″:5″,2‴-quaterselenophene.[44] The π-conjugated backbones of the molecules are

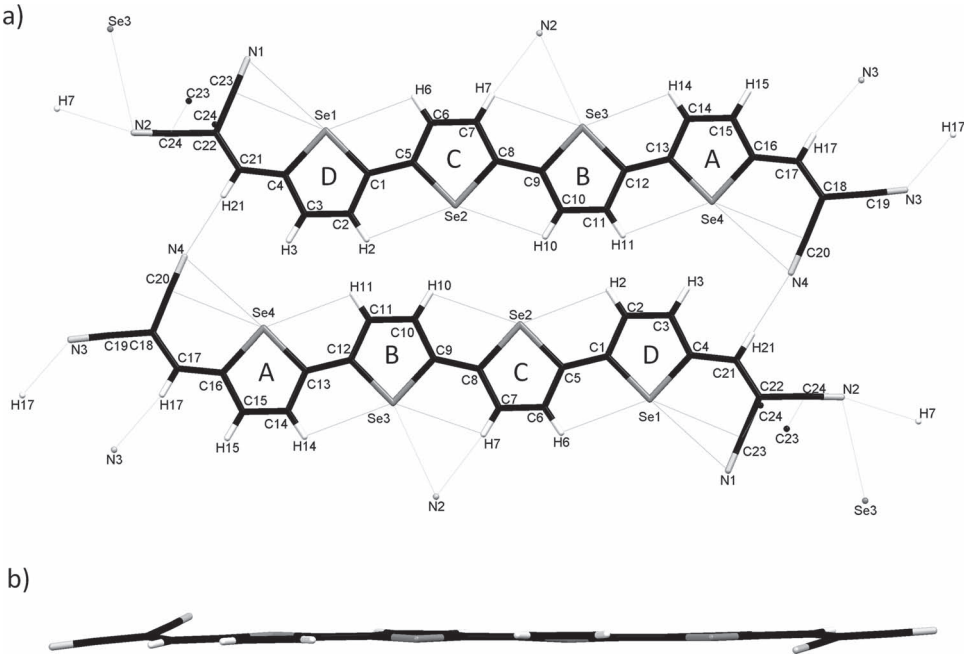

Figure 4. a) Molecular structure of **DCV4S** (front view) with atomic numbering scheme. Inter- and intramolecular short contact distances are depicted by gray lines, respectively. Torsion angles between adjacent selenophene rings: A-B 178.7°, B-C 175.5°, C-D 178.4°, N4-A 9.3°, D-N1 6.2°. b) Side view.

oriented parallel to one another, as it is seen in the view from the [010] direction (**Figure 6**). The intermolecular distances, "d", are 3.563 Å compared to 3.512 Å for **DCV4T**, indicating a slightly less compact packing and π–π stacking of the selenophene backbones due to the larger van der Waals radius of selenium compared to sulfur. In the perpendicular direction, the molecules (Figure 5) are lying in approximate coplanarity with a small offset between neighboring molecules (Δ = 1.085 Å; Figure 6). As in the case of **DCV4T**, weak non-classical hydrogen bonding interactions caused by the terminal nitrile

Table 3. Bond lengths [Å] in the oligoselenophene moiety in **DCV4S** single crystals (Se-C bond lengths are shown in bold).

N1	C23	1.141(4)	C9	Se3	**1.875(2)**
C23	C22	1.427(4)	C9	C10	1.367(3)
N2	C24	1.151(4)	C10	C11	1.405(3)
C24	C22	1.434(4)	C11	C12	1.366(3)
C22	C21	1.363(4)	C12	Se3	**1.880(2)**
C21	C4	1.425(3)	C12	C13	1.439(3)
C4	Se1	**1.883(2)**	C13	Se4	**1.874(2)**
C4	C3	1.381(4)	C13	C14	1.376(3)
C2	C3	1.410(3)	C14	C15	1.402(4)
C2	C1	1.379(3)	C15	C16	1.370(4)
C1	Se1	**1.880(2)**	C16	Se4	**1.892(2)**
C5	C1	1.439(2)	C16	C17	1.414(3)
C5	Se2	**1.875(2)**	C17	C18	1.357(4)
C6	C5	1.370(3)	C18	C19	1.437(3)
C6	C7	1.407(3)	C18	C20	1.439(4)
C7	C8	1.371(4)	C19	N3	1.147(3)
C8	Se2	**1.886(2)**	C20	N4	1.152(4)
C8	C9	1.445(3)			

Table 4. Short inter- (left) and intra- (middle and right) molecular contacts [Å], below the sum of the van der Waals radii, in **DCV4S** single crystals.

C23…C24[a)]	3.345	Se1…C23	3.116	Se3…H7	2.986
N2…Se3[b)]	3.428	Se1…N1	3.328	Se3…H14	2.952
N2…H7[c)]	2.689	Se1…H6	2.948	Se4…C20	3.147
N3…H17[d)]	2.504	Se2…H2	2.962	Se4…N4	3.319
N4…H21[e)]	2.526	Se2…H10	2.968	Se4…H11	2.967

Symmetry codes: [a)]–1 + x, y, z; [b)]1.5 + x, 1/2 - y, ½ + z; [c)]–1.5 + x, 1/2 - y, –1/2 + z; [d)]–3 + x, y, 1 + z; [e)]1 – x, 1 – y, 1 – z.

residues seem to be the main driving forces for the parallel ordering of the π-conjugated system in **DCV4S**. This explains the same packing features of both compounds. In summary, the general packing pattern is controlled by the DCV groups while the intermolecular π–π distances are increased by incorporation of selenium into the conjugated backbone.

2.6. Photovoltaic Performance

Due to the low-lying HOMO energy level and the possible n-type character **DCV3S** was not used for solar cell fabrication. **DCV4S** and **DCV5S**, however, were implemented as donor material in combination with fullerene C_{60} as electron acceptor, both in planar heterojunction (PHJ) and in bulk-heterojunction (BHJ) solar cells. The devices were fabricated by vacuum sublimation on glass substrates coated with indium tin oxide (ITO). For the PHJ devices, the following layer sequence was used: ITO coated glass, 15 nm C_{60} as acceptor, 6 nm or 10 nm **DCV4S** or **DCV5S** as donor, 5 nm undoped 9,9-bis[4-(*N*,*N*-bis-biphenyl-4-ylamino)-phenyl]-9*H*-fluorene (BPAPF), 50 nm BPAPF doped with 10 wt% NDP9 as hole transporting layer (HTL), 1 nm NDP9, 50 nm gold as top electrode. For the BHJ devices, a 20 nm or 30 nm mixed donor-acceptor layer was used instead of the pristine donor layer. This layer was prepared by co-evaporation of the respective donor (**DCV4S** or **DCV5S**) and C_{60} as acceptor on a heated substrate. The device with **DCV4S** was fabricated at a substrate temperature of 70 °C and a blend ratio of 1:1, while **DCV5S** was deposited at 90 °C with a blend ratio of 2:1. These conditions had turned out to be optimal for the corresponding oligothiophenes.[26,27]

The current density-voltage (*J*–*V*) curves of the PHJ and BHJ devices and the external quantum efficiency (EQE) spectra are shown in Figure 6 and **Figure 7**, respectively. The photovoltaic parameters are summarized in **Table 5**. The dark curves in PHJ solar cells showed very good rectification behavior, while larger leakage currents were observed in BHJ devices.

For both device architectures, the layer thicknesses do not significantly influence the overall device efficiencies. The short circuit current density (J_{SC}) increases with increased layer thickness, but the fill factor (FF) decreases leading to an almost unchanged overall efficiency. **DCV5S** gave better PCEs (PHJ: 3.4%; BHJ: 2.6%) compared to **DCV4S** (PHJ: 2.4%; BHJ: 1.7%). All devices showed a high V_{OC}, as V_{OC} is generally determined by the energetic difference between the LUMO of the acceptor C_{60} and the HOMO of the donor.[45] In **DCV4S** and **DCV5S**-based PHJ devices, the V_{OC} decreases from 0.95 V to about 0.91 V. In this architecture, the change of V_{OC} represents in a first approximation the HOMO energy level difference between the two donor materials in the solid state.[46] This difference can

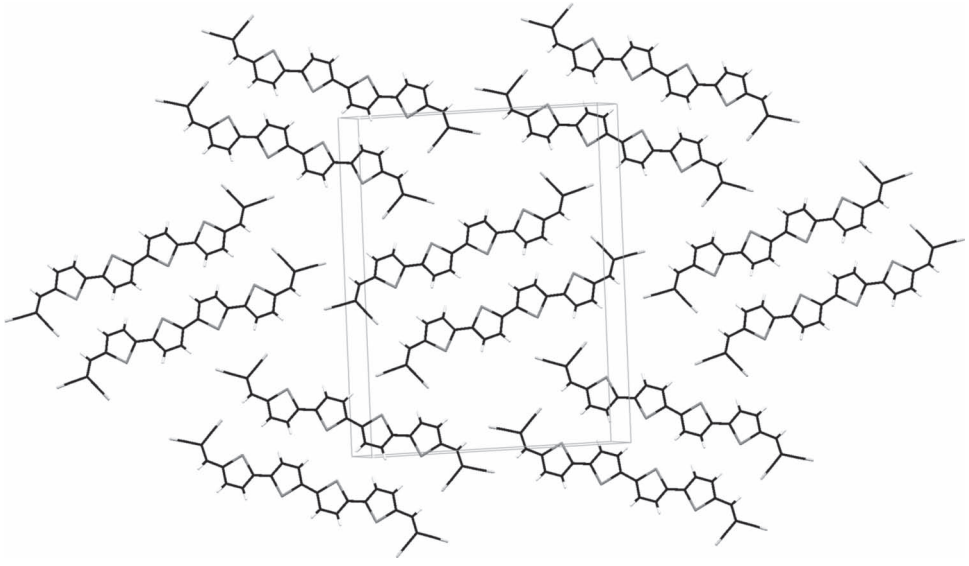

Figure 5. Molecular packing of **DCV4S** in the single crystal viewed from the direction normal to the (9 3 21) plane.

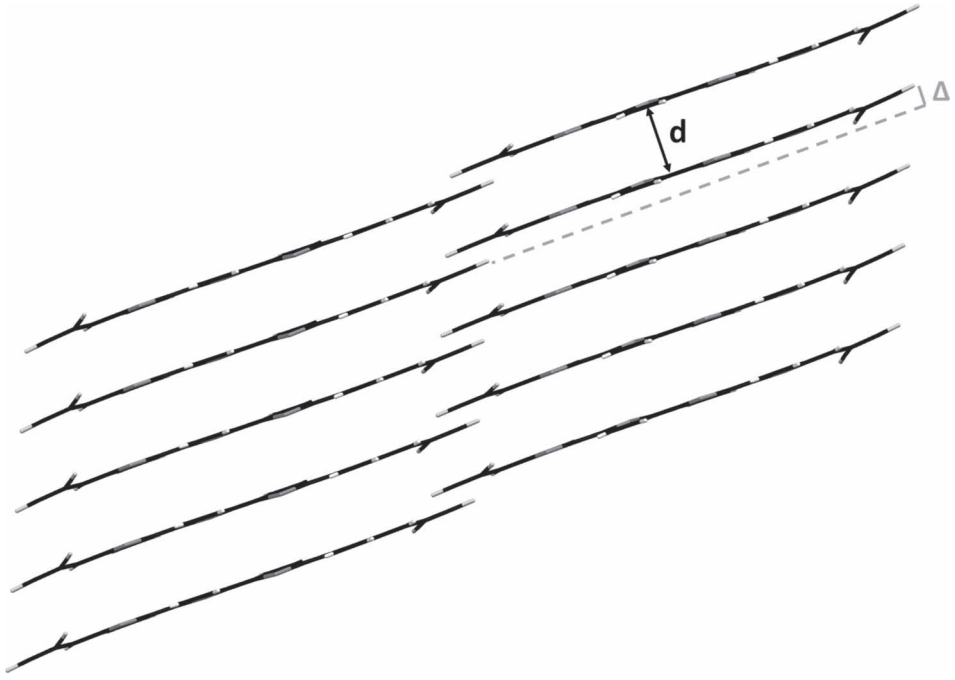

Figure 6. Molecular packing of **DCV4S** in the single crystal view from the [010] direction showing the π–π stacking [d] of the molecules.

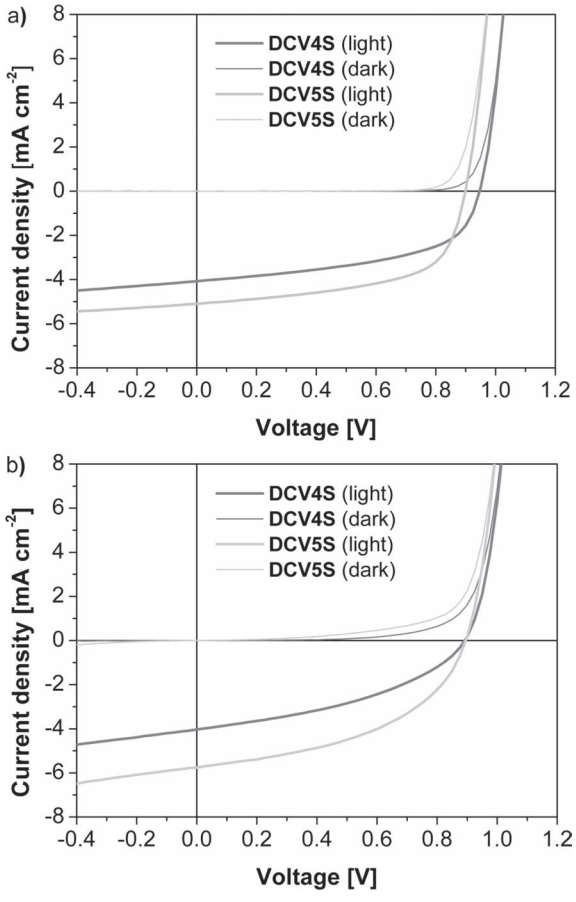

Figure 7. *J–V* characteristics of a) planar heterojunction solar cells (6 nm donor layer) and b) bulk-heterojunction solar cells (20 nm bulk layer) with **DCV4S** and **DCV5S** as donor materials.

also be expected from the electrochemically determined energy levels ($\Delta E_{HOMO} \approx 0.2$ eV) as shown in Table 2. One explanation for the deviation of the energetic shift could be that the latter values were obtained for single molecules in solution, whereas the values in the devices were shifted due to molecular packing in the solid state. Since the HOMO values of **DCV*n*S** are very similar to those of **DCV*n*T**, the V_{OC} values for the oligoselenophenes are comparable to those of the corresponding oligothiophenes.

In the PHJ devices, J_{SC} increased with increasing layer thickness from 6 to 10 nm. This result shows that the exciton diffusion length is larger than 6 nm in both materials. The PHJ solar cells with **DCV5S** showed slightly higher J_{SC} values of 7.1 mA cm^{-2}. This can be correlated to the EQE spectra of the **DCV5S** devices which are broad and red-shifted compared to **DCV4S**. The **DCV5S** spectra showed an onset at ≈800 nm reaching a maximum of ≈0.35, while the maximum for **DCV4S** lies below 0.3 with an onset at ≈750 nm (**Figure 8**a). Thus, more charge carriers are generated in the **DCV5S** device, leading to an increased photocurrent.

The PHJ devices with **DCV4S** showed lower FF and larger saturation values compared to the devices with **DCV5S**. Both effects originate from a voltage dependent photo-generated charge carrier recombination. One explanation could be an insufficient energetic LUMO offset between **DCV4S** and C_{60} leading to inefficient and voltage-dependent exciton separation at this interface.

For both compounds, the PHJ devices showed better PCEs than the BHJ devices. This difference in performance was mainly due to the slightly increased J_{SC} values and significantly higher FFs for the PHJ devices. This trend is in contrast to previous results with corresponding oligothiophenes in which BHJ devices outperformed PHJ solar cells.[27] All BHJ devices

Table 5. Photovoltaic parameters of PHJ and BHJ solar cells containing **DCV4S** and **DCV5S**.

Oligomers	Device structure	Substrate temperature [°C]	Layer thickness [nm]	$J_{SC,ap,100}$ [a)] [mA cm^{-2}]	V_{OC} [V]	FF	Saturation [b)]	Incident light intensity [mW cm^{-2}]	PCE [%]
DCV4S	PHJ	r.t.	6	4.8	0.95	0.53	1.24	96	**2.4**
DCV4S	PHJ	r.t.	10	5.3	0.95	0.47	1.30	96	**2.4**
DCV5S	PHJ	r.t.	6	6.3	0.90	0.59	1.16	92	**3.3**
DCV5S	PHJ	r.t.	10	7.1	0.91	0.53	1.20	92	**3.4**
DCV4S	BHJ	70	20	4.6	0.89	0.41	1.44	97	**1.7**
DCV4S	BHJ	70	30	4.8	0.88	0.39	1.43	97	**1.6**
DCV5S	BHJ	90	20	6.1	0.90	0.47	1.48	105	**2.6**
DCV5S	BHJ	90	30	6.4	0.89	0.45	1.45	105	**2.6**

[a)]Measured with mask; [b)]Defined as $J(-1\ V)/J_{SC}$.

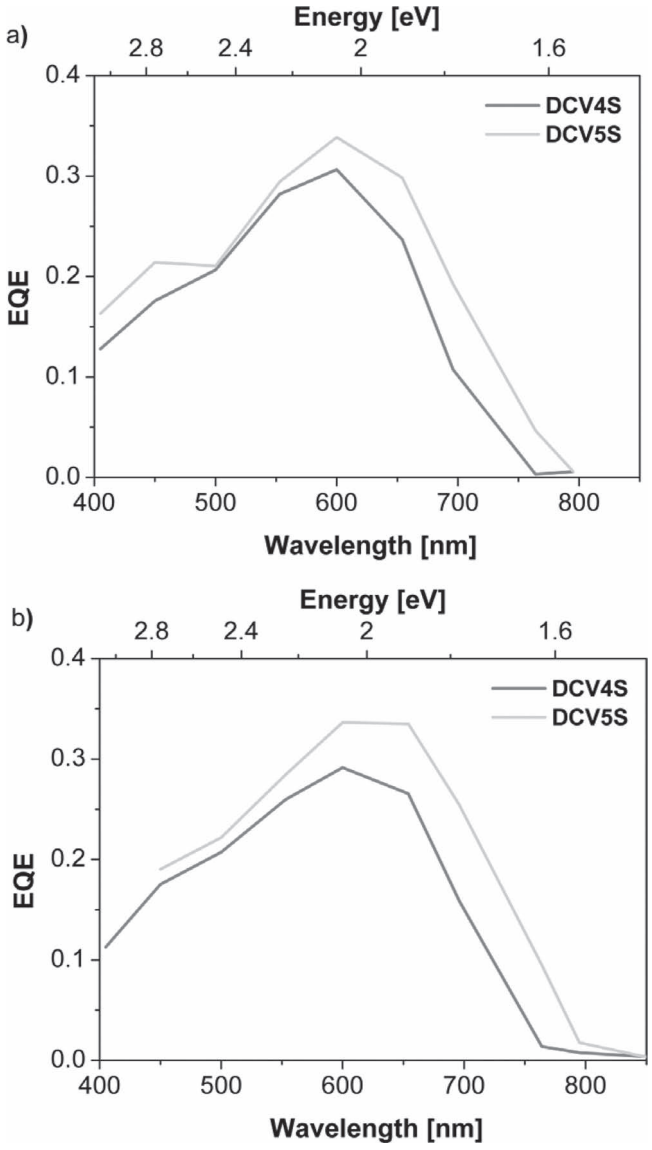

Figure 8. External quantum efficiency (EQE) spectra of a) PHJ solar cells and b) BHJ devices with **DCV4S** and **DCV5S**.

showed non-optimal rectifying behavior. Increasing the blend layer thickness from 20 to 30 nm only slightly affected the photovoltaic parameters of the BHJ solar cells, which are summarized in Table 4. One explanation for both effects could be a strong crystallization and phase separation of the oligoselenophenes and C_{60} when deposited on a heated substrate. As a consequence, the generated photocurrent is strongly limited by exciton diffusion, leading to stagnation of J_{SC} with increasing blend layer thickness. At the same time, comparably low FF and high saturation values point towards non-optimal charge carrier transport in these particular blend layers.

Compared to the previously investigated oligothiophenes **DCV4T** and **DCV5T**, the PHJ device efficiencies (6 nm donor layer) of **DCV4S** and **DCV5S** are higher. In the case of the tetramers, the PCE of **DCV4S** (2.4%) is twice as high as the PCE for **DCV4T** (1.2%).[27] This is mainly a consequence of the much higher J_{SC} (5.2 vs 2.9 mA cm^{-2}). For the pentamers, the efficiency increases from 2.6% for **DCV5T** to 3.4% for **DCV5S** due to both, higher J_{SC} and FF values.

In BHJ devices (20 nm active layer) the PCE for **DCV4S** (1.7%) is very similar to that of **DCV4T** (1.5%).[26] However, a considerable decrease of the efficiency was observed for **DCV5S** (2.6%) compared to **DCV5T** (3.9%).[27] The main reason for this decrease is the lower FF (0.45 for **DCV5S** vs. 0.61 for **DCV5T**), which could be a result of less efficient charge carrier extraction.

In order to improve the device performance, further detailed studies are necessary on the optimization of substrate temperature and fabrication conditions. In our previous investigation, we also observed that the efficiency of DCV-endcapped thiophene-selenophene co-oligomers dropped with increasing selenophene content due to poorer phase separation.[28]

3. Conclusion

We reported on the synthesis of a series of longer oligoselenophenes with terminal acceptor groups (**DCV*n*S**). The influence of selenium in the conjugated oligomers on optoelectronic properties and solar cell performance has been explored in detail and compared with the corresponding oligothiophenes **DCV*n*T**. Thermal, optical and electrochemical properties of

DCV*n*S exhibited similar chain length dependence as the corresponding oligothiophenes. Red-shifted absorption bands and lowering of the bandgap were observed for **DCV*n*S** in comparison with **DCV*n*T**. The replacement of sulfur by selenium led to a lowering of the LUMO energy level, while the HOMO level stayed relatively unaffected. The single crystal structure analysis of tetramer **DCV4S** confirmed the important role that the DCV groups play for molecular ordering, whereas the introduction of selenium resulted in increased intermolecular distances compared to **DCV4T**. Oligomers **DCV4S** and **DCV5S** were implemented as donor materials in vacuum-processed PHJ and BHJ solar cells with C_{60} as acceptor. This is the first time that longer oligoselenophenes were used as donor materials in small molecule organic solar cells (SMOSC). In PHJ devices, the oligoselenophenes showed higher PCEs than their thiophene analogs, the best efficiency being 3.4% for **DCV5S**. In BHJ devices, the PCE for **DCV5S** was lower than for **DCV5T**, but there is still room for improvement by optimization of the fabrication conditions. Nevertheless, these results demonstrate the successful application of acceptor-functionalized oligoselenophenes as donor materials for efficient SMOSC.

4. Experimental Section

Instruments and Measurements: NMR spectra were recorded on a Bruker AMX 500 (^{1}H NMR: 500 MHz, ^{13}C NMR: 125 MHz) or an Avance 400 spectrometer (^{1}H NMR: 400 MHz, ^{13}C NMR: 100 MHz) at 25 °C unless otherwise noted. Chemical shift values (δ) are expressed in parts per million using residual solvent protons (^{1}H NMR, δ_H = 7.26 for $CDCl_3$, δ_H = 5.32 for CD_2Cl_2, δ_H = 5.92 for $C_2D_2Cl_4$, δ_H = 2.50 for DMSO-d_6; ^{13}C NMR, δ_C = 77.0 for $CDCl_3$, δ_C = 53.84 for CD_2Cl_2) as internal standard. The splitting patterns are designated as follows: s (singlet), d (doublet), t (triplet), and m (multiplet). The assignments are Sel-H (selenophene protons), -CHO (aldehyde protons), DCV-H (dicyanovinyl protons). Melting points were determined using a Mettler Toledo DSC 823^e and were not corrected. Elemental analyses were performed on an Elementar Vario EL. Thin layer chromatography was carried out on aluminum plates, pre-coated with silica gel, Merck Si60 F_{254}. Preparative column chromatography was performed on glass columns packed with silica gel, Merck Silica 60, particle size 40–63 µm. EI mass spectra were recorded on a Varian Saturn 2000 GC-MS and MALDI-TOF mass spectra on a Bruker Daltonics Reflex III.

X-ray diffraction data of a dark-red **DCV4S** single crystal were collected in a stream of nitrogen at 100(2) K on a Bruker APEX-II CCD area detector diffractometer using graphite-monochromated Mo Kα radiation. Absorption correction based on a semi-empirical method was performed with the SADABS algorithm.[47] The structure was solved by direct methods with SHELXS-97,[48] revealing all atoms of the selenophene backbone. Additional atoms were located from difference Fourier maps during refinement on F^2 with SHELXL-97.[48] In the structure, voids in the asymmetric unit with a volume of ca. 97 Å^3 are present. These voids represent ca. 17% of the overall volume and are filled with heavily disordered **DCV4S** molecules, clearly discernible from the smeared electron density (maximum electron density within the voids 11.2 e$^-$). It was not possible to resolve this disorder satisfactorily. Therefore, all electron density associated with peaks in these voids was eventually omitted by applying the PLATON/SQUEEZE option.[49] For the final model, all non-H atoms were refined anisotropically. H atoms were placed in calculated positions riding the parent C atom with C−H distance constraints of 0.95 Å, and with U_{iso}(H) = 1.2U_{eq}(C). **DCV4S**: $C_{24}H_{10}N_4Se_5$, M_r = 670.20, dark-red lath, 0.65 × 0.24 × 0.10 mm^3, monoclinic, $P2_1/n$, a = 3.9203(1) Å, b = 27.6816(9) Å, c = 22.7887(7) Å, β = 93.181(2) °, V = 2469.22(13) Å^3, Z = 4, μ = 5.961 mm^{-1} , dx = 1.803 g·cm^{-3}, T = 100(2) K. 49820 reflections collected (θ_{max} = 38.1°) and merged to 13421 independent data (R_{int} = 0.050); final R indices: $R_1(I > 2\sigma(I))$ = 0.0481, wR_2 (all) = 0.1109.

Detailed crystallographic data for the structure of **DCV4S** have been deposited with the Cambridge Crystallographic Data Centre as supplementary publication CCDC 874137.

Optical measurements in solution were carried out in 1 cm cuvettes with Merck Uvasol grade solvents. Absorption spectra were recorded on a Perkin Elmer Lambda 19 spectrometer and corrected fluorescence spectra were recorded on a Perkin Elmer LS 55 fluorescence spectrometer. Cyclic voltammetry experiments were performed with a computer-controlled Autolab PGSTAT30 potentiostat in a three-electrode single-compartment cell with a platinum working electrode, a platinum wire counter electrode, and an Ag/AgCl reference electrode. All potentials were internally referenced to the ferrocene/ferrocenium couple.

Thin Film and Device Fabrication: Thin films and heterojunction solar cell devices were prepared by thermal vapor deposition in ultra high vacuum at a base pressure of 10^{-7} mbar onto the substrate at room temperature. Thin films for absorption and emission measurements were prepared on quartz substrates, solar cells on tin-doped indium oxide (ITO) coated glass (Thin Film Devices, USA, sheet resistance of 30 Ω sq^{-1}). Layer thicknesses were determined during evaporation by using quartz crystal monitors calibrated for the respective material. The thin films prepared for absorption and emission measurements are approximately 30 nm thick. Thin film absorption spectra were recorded on a Shimadzu UV-2101/3101 UV–Vis spectrometer. The thin film emission spectra were recorded with an Edinburgh Instruments FSP920 fluorescence spectrometer. Planar heterojunction and bulk-heterojunction solar cells were prepared layer by layer without breaking the vacuum. The layer structure of the bulk-heterojunction solar cells is as follows: ITO/15 nm C_{60}/20 or 30 nm blend layer of respective **DCV*n*S** and C_{60} (ratio 1:1 or 2:1 in volume) prepared by co-evaporation on heated substrate (70 or 90 °C)/5 nm BPAPF/50 nm BPAPF doped with 10 wt% NDP9 (Novaled AG, Dresden, Germany)/1 nm NDP9/50 nm gold. The planar heterojunction devices were built up as follows: ITO/15 nm C_{60}/6 nm or 10 nm donor layer of respective **DCV*n*S**/5 nm BPAPF/50 nm BPAPF doped with 10 wt% NDP9 (purchased from Novaled AG, Dresden, Germany)/1 nm NDP9/50 nm gold. The dopant material NDP9 was purchased from the company Novaled AG, Dresden, Germany, and can be available by directly contacting the company.

Photovoltaic Characterization: *J–V* and EQE measurements were carried out in a glove box with nitrogen atmosphere. *J–V* characteristics were measured using a source-measure unit (Keithley SMU 2400) and an AM 1.5G sun simulator (KHS Technical Lighting SC1200). The intensity was monitored with a silicon photodiode (Hamamatsu S1337) which was calibrated at Fraunhofer ISE. The mismatch between the spectrum of the sun simulator and the AM 1.5G spectrum was not taken into account. For well defined active solar cell areas, aperture masks (2.76 mm^2) were used. Simple EQE measurements were carried out using the sun simulator in combination with color filters for monochromatic illumination. The illumination intensities were measured with a silicon reference diode (Hamamatsu S1337).

Materials: Dimethylformamide (DMF, Merck) was dried under reflux over phosphorous pentoxide (Merck). Dichloromethane (DCM), dichloroethane (DCE), ethanol (EtOH) and ethyl acetate were purchased from Merck and distilled prior to use. All synthetic steps were carried out under an argon atmosphere (except Knoevenagel condensations). β-Alanine, *N*-bromosuccinimide (NBS), phosphoryl chloride, sodium hydrogencarbonate and sodium sulfate were purchased from Merck. $Pd(PPh_3)_2Cl_2$ and $Pd(PPh_4)_3$ were purchased from Acros. 2,5-dibromoselenophene,[28] 2,2′:5′,2″-terselenophene **1**,[5] 2,5-bis(trimethylstannyl)selenophene **3**,[50] 2-((5-bromoselenophen-2-yl)-methylene)malononitrile **4**[28] and 2,2′-biselenophene-5-carbaldehyde **5**[5] were synthesized according to literature procedures.

[2,2′:5′,2″-Terselenophene]-5,5″-dicarbaldehyde **(2)**: DMF (2.29 g, 31.3 mmol) was dissolved under argon in DCE (30 mL) and $POCl_3$ (4.72 g, 30.8 mmol) was slowly added at 0 °C. The mixture was stirred at r.t. for 2 h. It was added to a solution of 2,2′:5′,2″-terselenophene **1** (595 mg, 1.53 mmol) in DCE (30 mL) and the resulting red mixture was

refluxed for 5 d. A sat. $NaHCO_3$ solution (150 mL) was added and the mixture was stirred for 1.5 h. It was extracted with DCM (5 × 200 mL). The combined organic layers were dried over Na_2SO_4 and the solvent was removed. The crude product was purified by column chromatography (flash silica; monoaldehyde eluted with DCM, dialdehyde eluted with DCM/ethyl acetate 8:2). The pure product **2** (426 mg, 0.957 mmol, 63%) was obtained as an orange solid. Melting point (Mp.) 215 °C; ^{1}H NMR (400 MHz, $CDCl_3$, δ): 9.76 (s with ^{77}Se-satellites, $^3J_{Se\text{-}H}$ = 4.6 Hz, 2H, -CHO), 7.90 (d, ^3J = 4.0 Hz, 2H, Sel-H-4,4''), 7.40 (s, 2H, Sel-H-3',4'), 7.38 (d, ^3J = 4.0 Hz, 2H, Sel-H-3,3''); ^{13}C NMR (100 MHz, $CDCl_3$, δ): 184.14, 153.60, 148.71, 145.20, 140.43, 130.37, 128.02; MS (MALDI-TOF, *m/z*): [M^+] = calcd. for $C_{14}H_8O_2Se_3$, 445.8; found 445.9; Anal. calcd. for $C_{14}H_8O_2Se_3$: C 37.78, H 1.81; found: C 38.03, H 2.12.

2,2'-([2,2':5',2''-Terselenophene]-5,5''-diylbis(methanylylidene))-dimalononitrile **(DCV3S)**: [2,2':5',2''-Terselenophene]-5,5''-dicarbaldehyde **2** (392 mg. 0.881 mmol), malononitrile (400 mg, 6.05 mmol) and β-alanine (10.8 mg, 0.121 mmol) were dissolved in a DCE/EtOH mixture (75 mL, 2:1 v/v) and the mixture was refluxed for 43 h. The mixture was cooled to r.t. and the solvent was reduced to half of its volume. The resulting solid was filtered off and washed thoroughly with ethanol, methanol and diethyl ether to obtain 390 mg of crude product. It was recrystallized from chlorobenzene (80 mL) and the resulting blackish crystals were filtered off, washed with ethanol and methanol and dried in high vacuum. 343 mg (0.634 mmol, 72%) of pure product **DCV3S** was obtained. Mp. 282 °C; ^{1}H NMR (500 MHz, DMSO-d_6, 360 K, δ): 8.55 (s, 2H, DCV-H), 8.11 (dd, ^3J = 4.5 Hz, ^4J = 0.5 Hz, 2H, Sel-H-4,4''), 7.78 (s, 2H, Sel-H-3',4'), 7.68 (d, ^3J = 4.5 Hz, 2H, Sel-H-3,3''); ^{13}C NMR (125 MHz, DMSO-d_6, 360 K, δ): 154.28, 154.12, 144.54, 144.10, 138.55, 131.56, 128.21, 113.68, 113.41, 74.83; MS (MALDI-TOF, *m/z*): [M^+] calcd. for $C_{20}H_8N_4Se_3$, 543.8; found: 543.9; Anal. calcd. for $C_{20}H_8N_4Se_3$: C 44.39, H 1.49, N 10.35; found: C 44.19, H 1.62, N 10.45.

2,2'-([2,2':5',2'':5'',2'''-Quaterselenophene]-5,5'''-diylbis(methanylylidene))dimalononitrile **(DCV4S)**: In a Schlenk tube, 5,5'-bis(trimethylstannyl)-2,2'-biselenophene **3** (396 mg, 0.676 mmol) and 2-((5-bromoselenophen-2-yl)methylene)malononitrile **4** (482 mg, 1.69 mmol) were dissolved in dry DMF (6 mL) and the solution was degassed. $Pd(PPh_3)_2Cl_2$ (23.5 mg, 33.5 µmol) was added, the solution was degassed again and stirred at 80 °C for 3 d. The solution was cooled to r.t. and the resulting solid was filtered off. It was washed with THF and methanol and dried in high vacuum to obtain **DCV4S** as a green solid (364 mg, 0.543 mmol, 80%). The compound was further purified by Soxhlet extraction with chlorobenzene for 3 weeks. Mp. 358 °C; ^{1}H NMR (500 MHz, DMSO-d_6, 360 K, δ): 8.54 (s, 2H, DCV-H), 8.11 (d, ^3J = 4.5 Hz, 2H, Sel-H), 7.75 (d, ^3J = 4.5 Hz, 2H, Sel-H), 7.64 (d, ^3J = 4.5 Hz, 2H, Sel-H), 7.55 (d, ^3J = 4.5 Hz, 2H, Sel-H); MS (MALDI-TOF, *m/z*): [M^+] calcd. for $C_{24}H_{10}N_4Se_4$: 671.8; found: 671.4; Anal. calcd. for $C_{24}H_{10}N_4Se_4$: C 43.01, H 1.50, N 8.36; found: C 43.33, H 1.71, N 8.55.

5'-Bromo-2,2'-biselenophene-5-carbaldehyde **(6)**: 2,2'-biselenophene-5-carbaldehyde **5** (1.29 g, 4.47 mmol) was dissolved in DMF (10 mL) and NBS (800 mg, 4.49 mmol) was dissolved in 5 mL DMF. The solutions were put in the freezer for 3 h. They were mixed and put back in the freezer for 3 d. The resulting crystals were filtered off and washed with methanol to obtain orange crystals (780 mg). The filtrate was put in the freezer over the weekend. The resulting precipitate was filtered off and another 280 mg of a yellow solid were obtained. Water was added to the filtrate and the mixture was extracted with DCM (3 × 25 mL). The combined organic layers were washed with water (3 × 20 mL), dried over Na_2SO_4 and the solvent was removed. The resulting solid was washed with methanol and dried in high vacuum to afford 385 mg of a yellow solid. All fractions contained pure product **6** and were combined to obtain an overall yield of 1.45 g (3.94 mmol, 88%). Mp. 153 °C; ^{1}H NMR (400 MHz, CD_2Cl_2, δ): 9.71 (s, 1H, -CHO), 7.87 (d, ^3J = 4.0 Hz, 1H, Sel-H-4), 7.28 (d, ^3J = 4.0 Hz, 1H, Sel-H-3), 7.23 (d, ^3J = 4.0 Hz, 1H, Sel-H-3'), 7.17 (d, ^3J = 4.0 Hz, 1H, Sel-H-4'); ^{13}C NMR (100 MHz, $CDCl_3$, δ): 183.88, 153.47, 147.85, 140.12, 134.10, 128.92, 127.23, 117.92; EIMS (*m/z* (%)): 368 (100, M), 339 (16, M-CHO), 260 (32, M-CHO-Br); Anal. calcd. for $C_9H_5BrOSe_2$: C 29.46, H 1.37; found: C 29.58, H 1.41.

2-((5'-Bromo-2,2'-biselenophen-5-yl)methylene)malononitrile **(7)**: 5'-Bromo-2,2'-biselenophene-5-carbaldehyde **6** (1.40 g, 3.82 mmol), malononitrile (763 mg, 11.5 mmol) and β-alanine (33 mg, 0.37 mmol) were suspended in an ethanol/DCE mixture (1:1 v/v, 15 mL) and the mixture was stirred at 80 °C for 2 h. The resulting red crystals were filtered off, washed with methanol and dried in high vacuum to afford 1.51 g (3.63 mmol, 95%) of product **7**. Mp. 208 °C; ^{1}H NMR (400 MHz, CD_2Cl_2, δ): 7.87 (s, 1H, DCV-H), 7.77 (d, ^3J = 4.3 Hz, 1H, Sel-H), 7.29-7.26 (m, 3H, Sel-H); ^{13}C NMR (100 MHz, CD_2Cl_2, δ): 156.74, 154.04, 144.93, 144.79, 138.84, 135.21, 130.51, 127.62, 119.92, 114.71, 114.41, 77.14; EIMS (*m/z* (%)): 418 (100, M), 337 (21, M-Br); Anal. calcd. for $C_{12}H_5BrN_2Se_2$: C 34.73, H 1.21, N 6.75; found: C 34.89, H 1.31, N 6.80.

2,5-Bis(trimethylstannyl)selenophene **(8)**: 2,5-Dibromoselenophene (3.09 g, 10.7 mmol) was dissolved under argon in dry diethyl ether (50 mL) and the solution was cooled to −78 °C. *n*-BuLi (1.6 M in hexane, 14.0 mL, 22.3 mmol) was added dropwise within 10 min and the mixture was stirred below −70 °C for 50 min. Trimethyltin chloride (4.69 g, 23.5 mmol, dissolved in 5 mL diethyl ether) was added and stirring was continued for 1.5 h. The mixture was poured into a sat. $NaHCO_3$ solution (80 mL) and extracted with diethyl ether (100 mL). The combined organic layers were dried over Na_2SO_4 and the solvent was removed to obtain 4.78 g of an off-white solid. The crude product was washed with methanol to obtain **8** as white crystals (3.24 g, 7.09 mmol, 66%). ^{1}H NMR (400 MHz, $CDCl_3$, δ): 7.68 (s, 2H, Sel-H), 0.37 (s with Sn-satellites, $^2J_{H\text{-}Sn}$ = 56 Hz, 18 H, Sn-Me); ^{13}C NMR (100 MHz, $CDCl_3$, δ): 150.16, 138.68, −7.79; EIMS (*m/z* (%)): 444 (100, $[M\text{-}CH_3]^+$); Anal. calcd. for $C_{10}H_{10}SeSn_2$: C 26.30, H 4.41; found: C 26.42, H 4.30.

2,2'-([2,2':5',2'':5'',2''':5''',2''''-Quinqueselenophene]-5,5''''-diylbis(methanylylidene))-dimalononitrile **(DCV5S)**: In a Schlenk tube, 2,5-bis(trimethylstannyl)selenophene **8** (201 mg, 0.440 mmol), 2-((5-bromo-2,2-biselenophen-5-yl)methylene)malononitrile **7** (384 mg, 0.925 mmol) and $Pd(PPh_3)_4$ (27 mg, 23.4 µmol, 5 mol%) were dissolved in dry DMF (12 mL) and the solution was degassed. It was stirred at 80 °C for 20 h. The resulting solid was filtered off, washed with THF and methanol and dried in high vacuum to obtain 317 mg of a green solid. It was further purified by Soxhlet extraction with chlorobenzene for 4 d to afford 260 mg (0.325 mmol, 74%) of **DCV5S** as a green solid. Mp. 324 °C; ^{1}H NMR (500 MHz, $C_2D_2Cl_4$, 340K, δ): 7.74 (s, 2H, DCV-H), 7.72 (d, ^3J = 4.5 Hz, 2H, Sel-H), 7.42 (d, ^3J = 4.0 Hz, 2H, Sel-H), 7.27 (d, ^3J = 4.0 Hz, 2H, Sel-H), 7.23 (s, 2H, Sel-H-3'',4''), 7.21 (d, ^3J = 4.0 Hz, 2H, Sel-H); MS (MALDI-TOF, *m/z*): [M^+] calcd. for $C_{28}H_{12}N_4Se_5$: 799.7; found, 799.7). Anal. calcd. for $C_{28}H_{12}N_4Se_5$: C 42.08, H 1.51, N 7.01; found: C 42.08, H 1.60, N 6.89.

Acknowledgements

The authors would like to thank the German Ministry of Education and Research (BMBF) for financial support in the frame of project OPEG 2010.

Received: April 11, 2012
Published online: June 19, 2012

[1] S. S. Zade, N. Zamoshchik, M. Bendikov, *Acc. Chem. Res.* **2011**, *44*, 14.
[2] S. S. Zade, N. Zamoshchik, M. Bendikov, *Chem. Eur. J.* **2009**, *15*, 8613.
[3] S. S. Zade, M. Bendikov, *Chem. Eur. J.* **2008**, *14*, 6734.
[4] S. Millefiori, A. Alparone, *Synth. Met.* **1998**, *95*, 217.
[5] H. Nakanishi, S. Inoue, T. Otsubo, *Mol. Cryst. Liq. Cryst.* **1997**, *296*, 335.
[6] S. Inoue, H. Nakanishi, K. Takimiya, Y. Aso, T. Otsubo, *Synth. Met.* **1997**, *84*, 341.
[7] A. Patra, Y. H. Wijsboom, G. Leitus, M. Bendikov, *Chem. Mater.* **2011**, *23*, 896.

[8] L. Li, J. Hollinger, A. A. Jahnke, S. Petrov, D. S. Seferos, *Chem. Sci.* **2011**, *2*, 2306.
[9] Y. H. Wijsboom, A. Patra, S. S. Zade, Y. Sheynin, M. Li, L. J. W. Shimon, M. Bendikov, *Angew. Chem.* **2009**, *121*, 5551; *Angew. Chem. Int. Ed.* **2009**, *48*, 5443.
[10] M. Heeney, W. Zhang, D. J. Crouch, M. L. Chabinyc, S. Gordeyev, R. Hamilton, S. J. Higgins, I. McCulloch, P. J. Skabara, D. Sparrowe, S. Tierney, *Chem. Commun.* **2007**, 5061.
[11] A. Patra, Y. H. Wijsboom, S. S. Zade, M. Li, Y. Sheynin, G. Leitus, M. Bendikov, *J. Am. Chem. Soc.* **2008**, *130*, 6734.
[12] D. Bhattacharyya, K. K. Gleason, *J. Mater. Chem.* **2012**, *22*, 405.
[13] W.-H. Lee, S. K. Lee, S. K. Son, J.-E. Choi, W. S. Shin, K. Kim, S.-H. Lee, S.-J. Moon, I.-N. Kang, *J. Polym. Sci., Part A* **2012**, *50*, 551.
[14] S. D. Oosterhout, M. M. Wienk, M. Al-Hashimi, M. Heeney, R. A. J. Janssen, *J. Phys. Chem. C* **2011**, *115*, 18901.
[15] A. Maurano, C. G. Shuttle, R. Hamilton, A. M. Ballantyne, J. Nelson, W. Zhang, M. Heeney, J. R. Durrant, *J. Phys. Chem. C* **2011**, *115*, 5947.
[16] M. I. Ozkut, S. Atak, A. M. Onal, A. Cihaner, *J. Mater. Chem.* **2011**, *21*, 5268.
[17] D. S. Chung, H. Kong, W. M. Yun, H. Cha, H.-K. Shim, Y.-H. Kim, C. E. Park, *Org. Electron.* **2010**, *11*, 899.
[18] H. A. Saadeh, L. Lu, F. He, J. E. Bullock, W. Wang, B. Carsten, L. Yu, *ACS Macro Lett.* **2012**, *1*, 361.
[19] A. M. Ballantyne, L. Chen, J. Nelson, D. D. C. Bradley, Y. Astuti, A. Maurano, C. G. Shuttle, J. R. Durrant, M. Heeney, W. Duffy, I. McCulloch, *Adv. Mater.* **2007**, *19*, 4544.
[20] R. Yang, R. Tian, J. Yan, Y. Zhang, J. Yang, Q. Hou, W. Yang, C. Zhang, Y. Cao, *Macromolecules* **2004**, *38*, 244.
[21] F. Gao, Y. Cheng, Q. Yu, S. Liu, D. Shi, Y. Li, P. Wang, *Inorg. Chem.* **2009**, *48*, 2664.
[22] R. Li, X. Lv, D. Shi, D. Zhou, Y. Cheng, G. Zhang, P. Wang, *J. Phys. Chem. C* **2009**, *113*, 7469.
[23] K. A. Mazzio, M. Yuan, K. Okamoto, C. K. Luscombe, *ACS Appl. Mater. Interfaces* **2011**, *3*, 271.
[24] A. Mishra, P. Bäuerle, *Angew. Chem. Int. Ed.* **2012**, *51*, 2020; *Angew. Chem.* **2012**, *124*, 2060.
[25] S. Steinberger, A. Mishra, E. Reinold, E. Mena-Osteritz, H. Müller, C. Uhrich, M. Pfeiffer, P. Bäuerle, *J. Mater. Chem.* **2012**, *22*, 2701.
[26] R. Fitzner, C. Elschner, M. Weil, C. Uhrich, C. Körner, M. Riede, K. Leo, M. Pfeiffer, E. Reinold, E. Mena-Osteritz, P. Bäuerle, *Adv. Mater.* **2012**, *24*, 675.
[27] R. Fitzner, E. Reinold, A. Mishra, E. Mena-Osteritz, H. Ziehlke, C. Körner, K. Leo, M. Riede, M. Weil, O. Tsaryova, A. Weiß, C. Uhrich, M. Pfeiffer, P. Bäuerle, *Adv. Funct. Mater.* **2011**, *21*, 897.
[28] S. Haid, A. Mishra, C. Uhrich, M. Pfeiffer, P. Bäuerle, *Chem. Mater.* **2011**, *23*, 4435.
[29] A. Mishra, C. Uhrich, E. Reinold, M. Pfeiffer, P. Bäuerle, *Adv. Energy Mater.* **2011**, *1*, 265.
[30] S. Steinberger, A. Mishra, E. Reinold, J. Levichkov, C. Uhrich, M. Pfeiffer, P. Bäuerle, *Chem. Commun.* **2011**, *47*, 1982.
[31] S. Steinberger, A. Mishra, E. Reinold, C. M. Müller, C. Uhrich, M. Pfeiffer, P. Bäuerle, *Org. Lett.* **2010**, *13*, 90.
[32] D. Wynands, B. Männig, M. Riede, K. Leo, E. Brier, E. Reinold, P. Bäuerle, *J. Appl. Phys.* **2009**, *106*, 054509.
[33] K. Schulze, M. Riede, E. Brier, E. Reinold, P. Bäuerle, K. Leo, *J. Appl. Phys.* **2008**, *104*, 074511.
[34] K. Schulze, C. Uhrich, R. Schüppel, K. Leo, M. Pfeiffer, E. Brier, E. Reinold, P. Bäuerle, *Adv. Mater.* **2006**, *18*, 2872.
[35] C. Uhrich, R. Schüppel, A. Petrich, M. Pfeiffer, K. Leo, E. Brier, P. Kilickiran, P. Bäuerle, *Adv. Funct. Mater.* **2007**, *17*, 2991.
[36] H. Kong, D. S. Chung, I.-N. Kang, J.-H. Park, M.-J. Park, I. H. Jung, C. E. Park, H.-K. Shim, *J. Mater. Chem.* **2009**, *19*, 3490.
[37] C. M. Cardona, W. Li, A. E. Kaifer, D. Stockdale, G. C. Bazan, *Adv. Mater.* **2011**, *23*, 2367.
[38] D. R. Lide, *CRC Handbook of Chemistry and Physics*, 84 ed., Boca Raton, FL **2003**.
[39] H. O. Villar, P. Otto, M. Dupuis, J. Ladik, *Synth. Met.* **1993**, *59*, 97.
[40] Q. Xie, F. Arias, L. Echegoyen, *J. Am. Chem. Soc.* **1993**, *115*, 9818.
[41] J. Schatz, *Science of Synthesis*, Vol. *9*, Thieme Verlag, Stuttgart **2000**, p. 287.
[42] J. Schatz, *Science of Synthesis*, Vol. *9*, Thieme Verlag, Stuttgart **2000**, p. 423.
[43] A. Bondi, *J. Phys. Chem.* **1964**, *68*, 441.
[44] H. Nakanishi, S. Inoue, Y. Aso, T. Otsubo, *Synth. Met.* **1999**, *101*, 639.
[45] D. Cheyns, J. Poortmans, P. Heremans, C. Deibel, S. Verlaak, B. P. Rand, J. Genoe, *Phys. Rev. B* **2008**, *77*, 165332.
[46] C. Uhrich, D. Wynands, S. Olthof, M. K. Riede, K. Leo, S. Sonntag, B. Männig, M. Pfeiffer, *J. Appl. Phys.* **2008**, *104*, 043107.
[47] G. M. Sheldrick, *SADABS*. University of Göttingen, Germany **2008**.
[48] G. M. Sheldrick, *Acta Cryst. A* **2008**, *64*, 112.
[49] A. L. Spek, *Acta Cryst. D* **2009**, *65*, 148.
[50] D. J. Crouch, P. J. Skabara, M. Heeney, I. McCulloch, D. Sparrowe, S. J. Coles, M. B. Hursthouse, *Macromol. Rapid Commun.* **2008**, *29*, 1839.